Computers and Concrete, *Vol. 14, No. 4 (2014) 419-444*
DOI: http://dx.doi.org/10.12989/cac.2014.14.4.419

Long-term flexural cracking control of reinforced self-compacting concrete one way slabs with and without fibres

Farhad Aslani*[1], Shami Nejadi[2] and Bijan Samali[3]

[1]*Centre for Infrastructure Engineering and Safety, School of Civil and Environmental Engineering, University of New South Wales, Australia*
[2]*School of Civil and Environmental Engineering, University of Technology Sydney, Australia*
[3]*Institute for Infrastructure Engineering, University of Western Sydney, Australia*

(*Received April 23, 2014, Revised August 1, 2014, Accepted October 6, 2014*)

Abstract. In this study experimental result of a total of eight SCC and FRSCC slabs with the same cross-section were monitored for up to 240 days to measure the time-dependent development of cracking and deformations under service loads are presented. For this purpose, four SCC mixes are considered in the test program. This study aimed to compare SCC and FRSCC experimental results with conventional concrete experimental results. The steel strains within the high moment regions, the concrete surface strains at the tensile steel level, deflection at the mid-span, crack widths and crack spacing were recorded throughout the testing period. Experimental results show that hybrid fibre reinforced SCC slabs demonstrated minimum instantaneous and time-dependent crack widths and steel fibre reinforced SCC slabs presented minimum final deflection.

Keywords: self-compacting concrete; fibre-reinforced self-compacting concrete; crack control; time-dependent; flexural cracking; deformations

1. Introduction

Self-compacting concrete (SCC) can be placed and compacted under its own weight with little or no vibration and without segregation or bleeding. SCC is used to facilitate and ensure proper filling and good structural performance of restricted areas and heavily reinforced structural members. It has gained significant importance in recent years because of its advantages (Aslani and Nejadi 2012a,b). Recently, this concrete has gained wider use in many countries for different applications and structural configurations. SCC can also provide a better working environment by eliminating the vibration noise. Such concrete requires a high slump that can be achieved by superplasticizer addition to a concrete mix and special attention to the mix proportions. SCC often contains a large quantity of powder materials that are required to maintain sufficient yield value and viscosity of the fresh mix, thus reducing bleeding, segregation, and settlement. As the use of a large quantity of cement increases costs and results in higher temperatures, the use of mineral admixtures such as fly ash, blast furnace slag, or limestone filler could increase the slump of the

*Corresponding author, Research Fellow, Ph.D, E-mail: F.Aslani@unsw.edu.au

http://www.techno-press.org/?journal=cac&subpage=8 ISSN: 1598-8198 (Print), 1598-818X (Online)

concrete mix without increasing its cost (Aslani and Nejadi 2013a, b).

Fibre-reinforced self-compacting concrete (FRSCC) is a relatively recent composite material that combines the benefits of the SCC technology with the advantages of the fibre addition to a brittle cementitious matrix. It is a ductile material that in its fresh state flows into the interior of the formwork, filling it in a natural manner, passing through the obstacles, and flowing and consolidating under the action of its own weight. FRSCC can mitigate two opposing weaknesses: poor workability in Fibre-reinforced concrete (FRC) and cracking resistance in plain concrete (Aslani 2013; Aslani and Natoori 2013). The performance of reinforced concrete structures under sustained loads particularly in the post-cracking range is an important design consideration. If sections are designed according to strength requirements only, the behaviour of the structure under sustained service loads may be unsatisfactory. For example, at service loads, deflections of the member may be excessively large or the width of the cracks may be unacceptable, even though the degree of the safety against collapse is satisfactory. Service load behaviour depends primarily on the properties of the concrete and these are often not known reliably at the design stage. As mentioned in the design of concrete structures, it is necessary to check the serviceability of the structure in the post-cracking range. The behaviour in this range is complicated by the effects of several factors, which are difficult to assess from analytical considerations only. Of prime importance are the effects of tension stiffening, random development of primary and secondary cracks, and the degree of bond breakdown.

A well-established method to predict crack opening in RC/FRC members is still lacking in the literature. Analytical models have been proposed by some authors (Chen *et al*. 2011; Arici and Granata 2013; Vandewalle 2000; Tan *et al*. 1995; Chiaia *et al*. 2008) but more experimental research is needed to validate the proposed formulations. In fact, only few experimental researches on reinforced concrete beams quantitatively relate the crack development (width and spacing) to the fibres properties (Chiaia *et al*. 2008; Oh 1992; Balazs and Kovacs 2004). Other works confirmed the effectiveness of fibres in reducing crack openings, analysing the influence of fibres on tension stiffening (Abrishami and Mitchell, 1997; Bishoff 2003; Minelli *et al*. 2010; Tan and Saha 2005). The influence of fibres reinforcement on cracking behaviour of RC beams under sustained loads is a topic almost unexplored. In fact, to the best knowledge of the authors, to date only the works of Tan *et al*. (1995) and Tan and Saha (2005) are focused on this issue.

According to the existing literature, the increase in crack width occurs at a decreasing rate with time due to long-term or cyclic loading and this increase can be up to twice the initial value within a few years. However, under most conditions, the spacing of cracks does not change with time at constant levels of stress. The test results compiled show that, under sustained loads the increase in crack width is caused by shrinkage of the concrete and by the time-dependent change of curvature. They also found that, there was a breakdown of bond with sustained loading (Nejadi 2005).

Nejadi (2005) has conducted a comprehensive experimental and analytical research about the time-dependent development of conventional concrete (CC) members' flexural cracking and the effect of long-term on crack widths and crack spacing. Nejadi's (2005) test results show that in the beam specimens, the maximum crack width within the high moment region increased rapidly in the first few weeks of loading when the creep and shrinkage strain developed rapidly. The rate of increases in crack width in the beams with a high sustained load is greater than for beams with a lower sustained load. The crack width is directly dependent on crack spacing, as a consequence results in larger crack width in those specimens with a thicker concrete cover. In Nejadi's (2005) slab specimens, a comparison of the results in different regions with different moment levels shows that under sustained loads, maximum and minimum crack width are proportional to the

bending moment, and crack width increases linearly as the applied moment increases. Also, the largest increase in crack width occurs in those regions subjected to low levels of bending moment; because cracks take more time to develop.

Little information is available in the literature regarding the time-dependent development of SCC and FRSCC flexural cracking and the effect of long-term on crack widths and crack spacing. Following tests have been down for monitoring the long-term behaviour of SCC and FRSCC beams but no one consider long-term behaviour of SCC and FRSCC slabs.

Xiao-jie *et al*. (2008) have performed long-term experimental tests of SCC beams. The shrinkage strain of SCC increases as the age increases. The shrinkage strain curves converge after 6 months. Also, under the same environmental conditions, the shrinkage-time curve of SCC is very similar to that of CC. The shrinkage strain of SCC after one year is about 450×10^{-6}. The creep coefficient of reinforced SCC beams for deflection after 18 months is about 1.6, which is very close to the normal reinforced CC beams. Mazzotti and Savoia (2009) have performed set of long-term creep tests on reinforced SCC beams. The results show that the long-term behaviour of SCC is qualitatively similar to the case of CC, both in terms of total shrinkage and creep strains. The creep strain attains an almost constant increase rate (in the time log scale) after approximately 2 months from casting. Nevertheless, creep and shrinkage are much greater for the specific SCC evaluated in this study than in the case of normal-slump concrete (e.g. CC). Also, the long-term deflection rate of beams under flexure is almost constant (in the time log scale) after the same period of time. On the contrary, the tensile strain rate in concrete close to the transverse cracks reduces after a few months from loading, suggesting the crack opening stabilization.

Buratti *et al*. (2010) have conducted series of long-term experimental tests for FRSCC beams. The performed tests showed that the magnitude of the delayed deformation can be high, up to 150% of the instantaneous counterpart. The rate of delayed deformation increased at lower rates for the FRSCC beams than for the plain SCC beam containing standard reinforcing bars. In particular, the lowest long-term damage was obtained for the specimen containing a combination of steel fibres of different sizes and of synthetic fibres usually employed to reduce shrinkage.

2. Research Significance

The experimental results of a total of eight SCC and FRSCC slabs with the same cross-section were monitored for up to 240 days to measure the long-term development of cracking and deformations under service loads are presented. For this purpose, four SCC mixes – two plain SCC, two steel, two polypropylene, and two hybrid FRSCC slab specimens – are considered in the test program. In this study, all testing and measurement requirements are based on the Nejadi (2005) research study and we aimed to compare SCC and FRSCC experimental results with CC experimental results. The steel strains within the high moment regions, the concrete surface strains at the tensile steel level, deflection at the mid-span, crack widths and crack spacing were recorded throughout the testing period.

The major objectives of the experimental program were:

(a) To gain a better understanding of the mechanisms associated with SCC and FRSCC flexural cracking of slab, and the influence of those factors that affect the spacing and width of flexural cracks under long-term loading.

(b) To obtain benchmark, laboratory-controlled data to assist in the development of rational design-oriented procedures for the control of cracking and the calculation of crack widths on the time-dependent response of one-way slabs made by SCC and FRSCC.

3. Experimental Study

3.1 Materials

3.1.1 Cement

In this experimental study, shrinkage limited cement (SLC) corresponding to the ASTM C183-08 (2000) (AS 3972 2010) standard was used. SLC is manufactured from specially prepared Portland cement clinker and gypsum. It may contain up to 5% of AS 3972 approved additions. The chemical, physical, and mechanical properties adhere to the limiting value or permissible limits specified in AS 2350.2, 3, 4, 5, 8, and 11 (2006).

3.1.2 Fly Ash

It is important to increase the amount of paste in SCC because fly ash is an agent to carry the aggregates. Eraring fly ash (EFA) is a natural pozzolan. It is a fine cream/grey powder that is low in lime content. The chemical, physical, and mechanical properties of the EFA used adhere to the limiting value or permissible limits specified in ASTM C311-11b (2000) (ACI 232.2R-03 2004; AS 2350.2 2006; AS 3583.1, 2, 3, 5, 6, 12, and 13, 1998).

3.1.3 Ground Granulated Blast Furnace Slag

Granulated blast furnace slag (GGBFS) is another supplementary cementitious material that is used in combination with SLC. GGBFS used in the experiment originated in Boral, Sydney, and it conformed to ASTM C989-06 (2000) (ACI 233R-95 2000; and AS 3582.2 2001) specifications.

3.1.4 Aggregate

In this study, crushed volcanic rock (i.e., latite) coarse aggregate was used with a maximum aggregate size of 10 mm. Nepean river gravel with a maximum size of 5 mm and Kurnell Natural River sand fine aggregates were also used. The sampling and testing of aggregates were carried out in accordance with ASTM C1077-13 (2000) (AS 1141 2011; RTA 2006).

3.1.5 Admixtures

The superplasticiser, viscosity-modifying admixture, and high-range water-reducing agent were used in this study. The new superplasticiser generation Glenium 27 complies with AS 1478.1 (2000) type High Range Water Reducer (HRWR) and ASTM C494 (2000) types A and F are used. The Rheomac VMA 362 viscosity modifying admixture that used in this study is a ready-to-use, liquid admixture that is specially developed for producing concrete with enhanced viscosity and controlled rheological properties. Pozzolith 80 was used as a high-range water-reducing agent in the mixes. It meets AS 1478 (2000) Type WRRe, requirements for admixtures.

3.1.6 Fibres

In this study, two commercially available fibres, Dramix RC-80/60-BN type steel fibres and Synmix 65 type polypropylene (PP) fibres, were used. The mechanical, elastic and surface structure properties of the steel and PP fibres are summarized in Table 1.

3.2 Mixture proportions

One control SCC mixture (N-SCC) and three fibre-reinforced SCC mixtures were used in this

study. Fibre-reinforced SCC mixtures contain steel (D-SCC), PP (S-SCC), and hybrid (steel + PP) (DS-SCC) fibres. The content proportions of these mixtures are given in Table 2. These contents were chosen to attempt to keep compressive strength to a level applicable to construction. As shown in Table 2, cement, fly ash, GGBFS, water, fine and coarse aggregates, VMA, and high range water reducing agent constituents amount are same for four mixes. But, fibre amount and superplasticiser that are used in the mixes are different.

A forced pan type of mixer with a maximum capacity of 150 liters was used. The volume of a batch with fibres was kept constant at 50 liters. First, powders and sand are mixed for 10 s and water and superplasticiser are added and mixed for 110 s and the coarse aggregate is added and at the end fibres are added to the pan and mixed for 90 s.

Table 1 The physical and mechanical properties of fibres

Fibre type	Fibre name	Density (kg/m^3)	Length (*l*)	Diameter (*d*)	Aspect ratio (*l*/*d*)	Tensile strength (MPa)	Modulus of elasticity (GPa)	Cross-section form	Surface structure
Steel	Dramix RC-80/60-BN	7850	60	0.75	80.0	1050	200	Circular	Hooked end
Polipropylene (PP)	Synmix 65	905	65	0.85	76.5	250	3	Square	Rough

Table 2 The proportions of the concrete mixtures (based on SSD condition)

Constituents	N-SCC	D-SCC	S-SCC	DS-SCC
Cement (kg/m^3)	160	160	160	160
Fly Ash (kg/m^3)	130	130	130	130
GGBFS (kg/m^3)	110	110	110	110
Cementitious content (kg/m^3)	400	400	400	400
Water (lit/m^3)	208	208	208	208
Water cementitious Ratio	0.52	0.52	0.52	0.52
Fine aggregate (kg/m^3)				
Coarse Sand	660	660	660	660
Fine Sand	221	221	221	221
Coarse aggregate (kg/m^3)	820	820	820	820
Admixtures (lit/m^3)				
Superplasticiser	4	4.86	4.73	4.5
VMA	1.3	1.3	1.3	1.3
High range water reducing agent	1.6	1.6	1.6	1.6
Fibre content (kg/m^3)				
Steel	-	30	-	15
PP	-	-	5	3

3 Mechanical properties samples' preparation and curing conditions

We used six 150 mm × 300 mm cylindrical moulds for the determination of compressive and strength per each age, and three cylindrical moulds 150 mm × 300 mm are used for the determination of the modulus of elasticity per each age. The specimens are kept covered in a controlled chamber at 20 ± 2°C for 24 h until demoulding. Thereafter, the specimens are placed in water presaturated with lime at 20°C. These compressive strength and modulus of elasticity are tested at 3, 7, 14, 28, 56, and 91 days. For each test, separated specimens are used and surface of specimens are smoothed.

Three 75 mm × 75 mm × 280 mm prism molds are used for the determination of drying shrinkage. After demolding shrinkage specimens, all of them are stored in standard temperate moist curing conditions at the measuring laboratory for a minimum of 24 h prior to initial measurement. Five 100 mm × 200 mm cylinders are used for the determination of creep in one creep rig. The applied stress value was determined by the 40% of the 28 days compressive strength results. All shrinkage and creep specimens are hold in the drying room with suitably controlled temperature, humidity and air circulation. The temperature and relative humidity of the drying room was 23±2℃ and 50±5% respectively (Aslani and Nejadi 2012c,d,e).

3.4 Mechanical properties samples' test methods

The compressive strength test, performed on 150 mm × 300 mm cylinders, followed AS 1012.14 (1991) and ASTM C39 (2000) tests for compressive strength of cylindrical concrete specimens. The cylinders were loaded in a testing machine under load control at the rate of 0.3 MPa/s until failure. The modulus of elasticity test that followed the the AS 1012.17 (1997) and ASTM C469 (2000) was done to 150 mm × 300 mm cylinders.

The shrinkage test, performed on 75 mm × 75 mm × 280 mm prisms, followed AS 1012.13 (1992) determination of the drying shrinkage of concrete test method. The creep test is performed on five 100 mm × 200 mm cylinders in one creep rig, followed AS 1012.16 (1996) determination of creep of concrete cylinders in compression test method.

3.5 Properties of fresh concrete

The experiments required for the SCC are generally carried out worldwide under laboratory conditions. These experiments test the liquidity, segregation, placement, and compacting of fresh concrete. Conventional workability experiments are not sufficient for the evaluation of SCC. Some of the experiment methods developed to measure the liquidity, segregation, placement, and compaction of SCC are defined in the European guidelines (2005) and ACI 237R-07 (2007) for SCC, including specification, production and use as slump–flow, V-funnel, U-box, L-box and fill-box tests.

This study performed slump flow, T_{50cm} time, J-ring flow, V-funnel flow time, and L-box blocking ratio tests. In order to reduce the effect of loss of workability on the variability of test results, the fresh properties of the mixes were determined within 30 min after mixing. The order of testing is as follows: 1. Slump flow test and measurement of T_{50cm} time; 2. J-ring flow test, measurement of difference in height of concrete inside and outside the J-ring and measurement of T_{50cm} time; 3. V-funnel flow tests at 10 s T_{10s} and 5 min T_{5min}; and 4. L-box test (Aslani and Maia 2013).

3.6 Slab specimens preparation and test set up

A total of eight SCC and FRSCC slabs with the same cross-section and details were monitored for up to 240 days to measure the time-dependent development of cracking and deformations under service loads. A general view of the test specimens is shown in Fig. 1. The slab specimens were each nominally 3500 mm long by 400 mm wide. In all slabs the nominal distance from the soffit to the centroid of the main reinforcement was 25 mm. Slabs series were each reinforced with 4N12. Details of the cross-sections and reinforcement layouts for slab specimens are shown in Fig. 1. The parameter is varied in the tests, including the four SCC mixes – plain SCC, steel, polypropylene, and hybrid FRSCC. Details of the slab specimens are given in Table 3.

All slab specimens were subjected to different gravity loads, consisting of self-weight plus superimposed sustained loads via carefully constructed and arranged concrete blocks supported off the top (of the specimens). To provide the sustained loading, rectangular concrete blocks of predetermined size and weights were cast and weighed prior to the commencement of the test. The blocks were suitably arranged on the top surface of each specimen to achieve the desired sustained load level (see Fig. 1). Two sustained load levels were considered, namely 50% and 30% of the ultimate design load, and designated load conditions ‘a’ and ‘b’, respectively. The slab specimens were subjected to uniformly distributed sustained loads, UDL + self-weight. All measurements were taken within the high moment region, i.e. the middle third of the span for beams and for slabs where $M \geq 90\%$ Mmax. For long-term tests the loading arrangement and high moment regions are shown in Fig. 2.

Each of the specimens was moist cured for a period of 14 days and then subjected to a constant sustained load. To measure the steel strains in the critical moment regions (e.g. high moment regions, see Fig. 2), 8 electric resistance strain gauges were attached to one of the main reinforcement bars. The strain gauges were connected to a HBM amplifier. To measure the concrete surface strains, 8 electric resistance strain gauges were glued onto the side face of each specimen at the steel level. While a microscope with a magnification factor of 40 was used to measure the crack widths. The development, propagation, extent, and width of cracking were observed and recorded throughout the test. Deflection at mid-span was measured using a Linear Variable Displacement Transducer (LVDT).

The inside surface of the mould was cleaned and thinly coated with a concrete release agent to prevent adhesion of the concrete. The SCC was placed into the mould in equal layers until each surface layer became smooth. Sufficient concrete was placed into the top layer to overfill the mould, after which the surface was stripped off and finished with a steel trowel. To measure the concrete material properties, companion specimens were also cast in the form of cylinders and prisms at the same time. The companion specimens were exposed to the same environmental, curing, and drying conditions as the test specimens. Creep coefficient and shrinkage strain for four SCC mixes was obtained. The specimens were left in their moulds for 3 days, and then removed

Table 3 Details of slabs for short-term flexural tests

Specimen	No. of Bars	Bar Diam. (mm)	Steel Area (mm^2)	c_b (mm)	c_s (mm)	s (mm)
Slab-a	4	12	452	25	40	103
Slab-b	4	12	452	25	40	103

Fig. 1 General view of flexural long-term tests under load

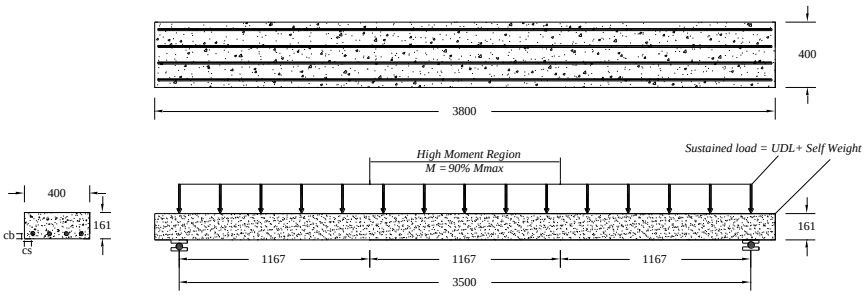

Fig. 2 Illustrative sustained loads slab specimens

from the mould and kept continuously moist by a thick covering of wet Hessian to minimise the loss of moisture from the concrete. After 14 days the covers and wet Hessian were removed, strain gauges were glued to the concrete surface and initial strain measurements were recorded. Slab specimens were uniformly loaded by the concrete blocks using wooden timbers as loading pads (Aslani *et al*. 2014).

4. Experimental Results

4.1 Properties of fresh concrete

The results of various fresh properties tested by the slump flow test (slump flow diameter and T_{50cm}); J-ring test (flow diameter); L-box test (time taken to reach 400 mm distance T_{400mm}, time taken to reach 600 mm distance T_{600mm}, time taken to reach 800 mm distance T_L, and ratio of heights at the two edges of L-box [H_2/H_1]); V-funnel test (time taken by concrete to flow through V-funnel after 10 s T_{10s}); the amount of entrapped air; and the specific gravity of mixes are given in Table 6. The slump flow test judges the capability of concrete to deform under its own weight against the friction of the surface with no restraint present. A slump flow value ranging from 500 to 700 mm for self-compacting concrete was suggested (European guidelines 2005). At a slump flow > 700 mm the concrete might segregate, and at < 500 mm, the concrete might have insufficient flow to pass through highly congested reinforcements.

All the mixes in the present study conform to the above range, because the slump flow of SCC is in the range of 600–700 mm. The slump flow time for the concrete to reach a diameter of 500 mm for all mixes was less than 4.5 s. The J-ring diameters were in the range of 560–655 mm. In addition to the slump flow test, a V-funnel test was also performed to assess the flowability and stability of SCC. V-funnel flow time is the elapsed time in seconds between the opening of the bottom outlet, depending when it is opened (T_{10s} and T_{5min}), and the time when light becomes visible at the bottom when observed from the top.

According to the European guidelines (2005), a period ranging from 6 to 12 s is considered adequate for SCC. The V-funnel flow times in the experiment were in the range of 7–11 s. The test results of this investigation indicated that all mixes met the requirements of allowable flow time. About V-funnel flow time test results for the N-SCC mix was 6 s and for the D-SCC was 7 s and for other fibre reinforced SCC mixes are blocked, obviously. The maximum size of coarse aggregate was restricted to 10 mm to avoid a blocking effect in the L-box for N-SCC mix. The gap between rebars in the L-box test was 35 mm. The L-box ratio H_2/H_1 for the N-SCC mix was above 0.8 which is, according to the European guidelines and, obviously, for other mixes is blocked. A total spread over 700 mm was measured and no sign of segregation or considerable bleeding in any of the mixtures was detected as the mixtures showed good homogeneity and cohesion (Aslani and Samali 2014).

Table 4 The SCC mixes workability characteristics

Workability characteristics	N-SCC	D-SCC	S-SCC	DS-SCC
Average spreading diameter (mm)	680	670	700	650
Flow time T_{50cm} (s)	2.7	3.8	2.5	3.2
Average J-Ring diameter (mm)	655	580	570	560
Flow time T_{50cm} J-Ring (s)	3.2	5	6	5
L-box test	0.87	Blocked*	Blocked	Blocked
Flow time V-funnel (s)	6	7	Blocked	Blocked
V-funnel at $T_{5minutes}$ (s)	4	5	Blocked	Blocked
Entrapped air (%)	1.3	1.2	1.2	1.0
Specific gravity (kg/m^3)	2340	2274	2330	2385

* Fibres are the main reason for blockage.

4.2 Compressive strength and modulus of elasticity

Table 5 presents the compressive strength and modulus of elasticity of the N-SCC, D-SCC, S-SCC, and DS-SCC mixes achieved at different ages. Compressive strength samples with fibre mixes are higher than N-SCC mix. The results indicate that the compressive strength of the DS-SCC mix at 91 days is 11%, 1%, and 8% higher than the N-SCC, D-SCC, and S-SCC mixes, respectively. Additionally, the results indicate that the modulus of elasticity of the DS-SCC mix at 91 days is 0.8%, 1%, and 1% higher than that of the N-SCC, D-SCC, and S-SCC mixes, respectively.

4.3 Deformation measurements results

Results of the shrinkage strain, creep strain, and total strain for all sets of loaded specimens are presented in Figs. 3-4.

After the commencement of drying, the shrinkage strain developed rapidly within the first two or three months and more than 50% of shrinkage occurred during this period. The maximum measured final shrinkage strain or N-SCC, D-SCC, S-SCC, DS-SCC, and N-CC mixtures were 870, 844, 823, 882, and 785 microstrains after 240 days. The maximum measured final shrinkage strain for SCC mixtures are not much different from each other. Also, the S-SCC mixture has the lowest final shrinkage strain that is 5.7%, 2.5%, and 7% lower than N-SCC, D-SCC, and DS-SCC mixtures.

The creep coefficient increased quickly for the first few weeks after loading, with almost 50% of creep occurring in the first 40 days after loading. The final creep coefficients for N-SCC, D-SCC, S-SCC, DS-SCC, and N-CC mixtures were 1.96, 1.86, 1.82, 1.45, and 1.49 after 240 days. There are very interesting results here the creep coefficient of DS-SCC mixture has same trend like N-CC. But, the other SCC mixtures have different behaviour.

The maximum creep coefficient is related to N-SCC without any fibres in the mixture. The creep coefficient of N-SCC mixture at age 240 days is 5%, 7%, 26%, and 24% higher than D-SCC, S-SCC, DS-SCC, and N-CC mixtures, respectively. Also, the creep coefficients of the D-SCC and S-SCC mixtures have close trend. The D-SCC mixture creep coefficient is just 2% higher than S-SCC mixture at age 240 days.

Table 5 Compressive strength and modulus of elasticity of SCC mixtures at different ages

Compressive strength (MPa)					Modulus of elasticity (GPa)				
Age (days)	N-SCC	D-SCC	S-SCC	DS-SCC	Age (days)	N-SCC	D-SCC	S-SCC	DS-SCC
3	12.45	18.50	13.65	14.30	3	25.23	24.45	25.36	3
7	21.80	25.30	22.50	26.30	7	27.84	26.57	27.87	7
14	29.05	34.30	32.45	38.10	14	32.24	29.14	29.68	14
28	33.30	38.00	38.10	45.00	28	35.39	35.76	35.76	28
56	40.60	50.50	42.90	50.75	56	35.58	36.44	36.32	56
91	46.40	51.15	47.65	52.00	91	37.79	37.58	37.47	91

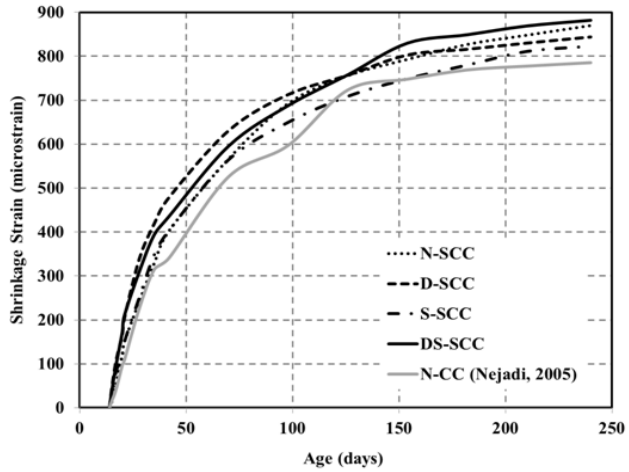

Fig. 3 The measured free shrinkage for unreinforced SCC and CC mixtures

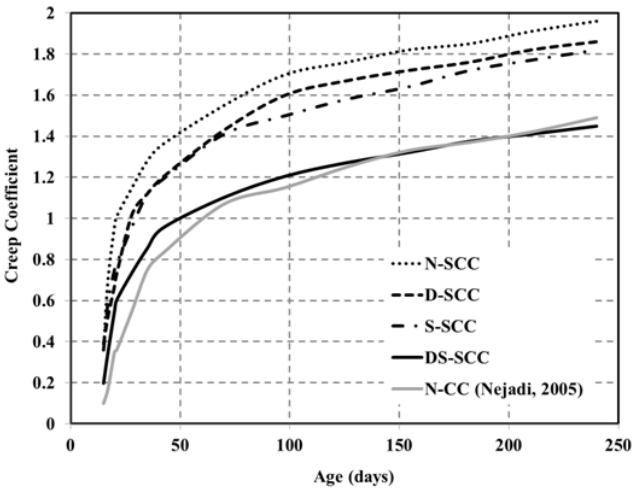

Fig. 4 The measured creep coefficient for SCC and CC mixtures

4.4 Long-term flexural cracking control test result of slabs

The slab lengths were divided into seven different regions namely; Region 1 ($M \geq 0.99Mmax$), Region 2 ($0.99Mmax > M \geq 0.9Mmax$), Region 3 ($0.9Mmax > M \geq 0.8Mmax$), Region 4 ($0.8Mmax > M \geq 0.7Mmax$), Region 5 ($0.7Mmax > M \geq 0.6Mmax$), Region 6 ($0.6Mmax > M \geq 0.5Mmax$) and Region 7 ($M < 0.5Mmax$). The development, extent and width of cracks were observed and measured within Regions 1 to 6 immediately after the first loading and during the remainder of the test period.

4.4.1 N-SCC slab series

To compare the maximum crack width located in different regions with different moment

levels, the measured maximum and average crack widths at commencement of the test (t = 0) and at the end (t = 240 days) for slabs N-SCC-a and N-SCC-b are presented in Table 6. The results from suggest that the largest percentage increase in crack width is in those regions subjected to low levels of bending moment, because the cracks take more time to develop. The visible cracks were developed at age 14 days where the primary crack pattern was established at first loading of slabs. The measured maximum instantaneous crack widths within Region 2, were 0.10 mm and

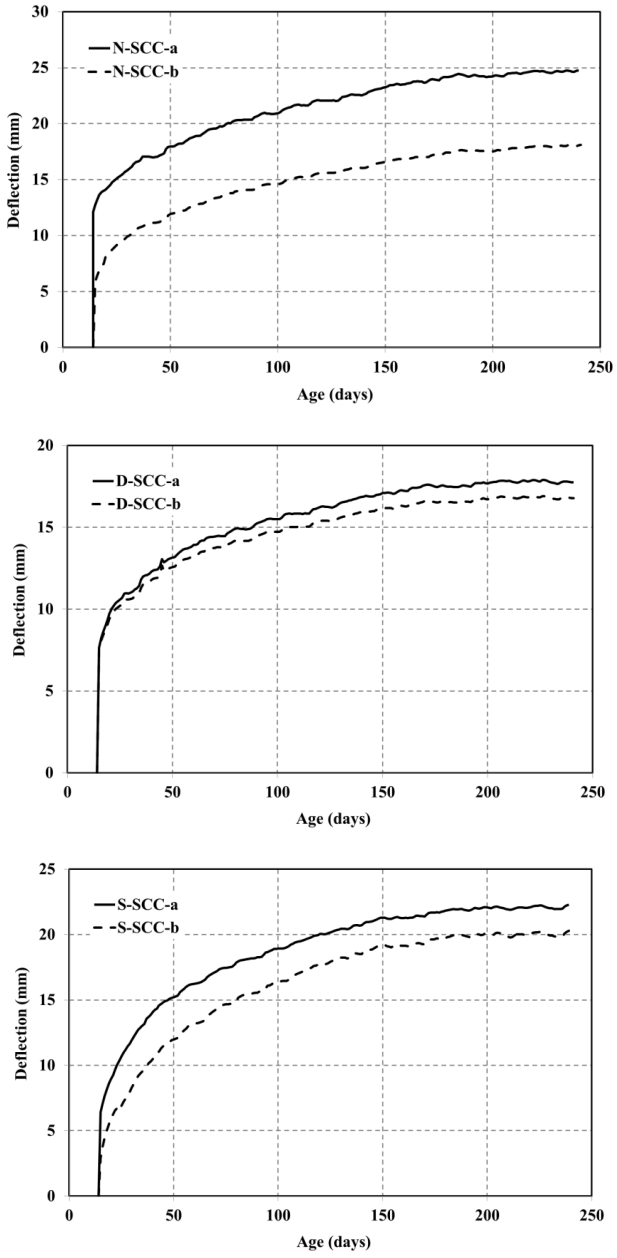

Fig. 5 Deflection of slabs SCC and N-CC slab series

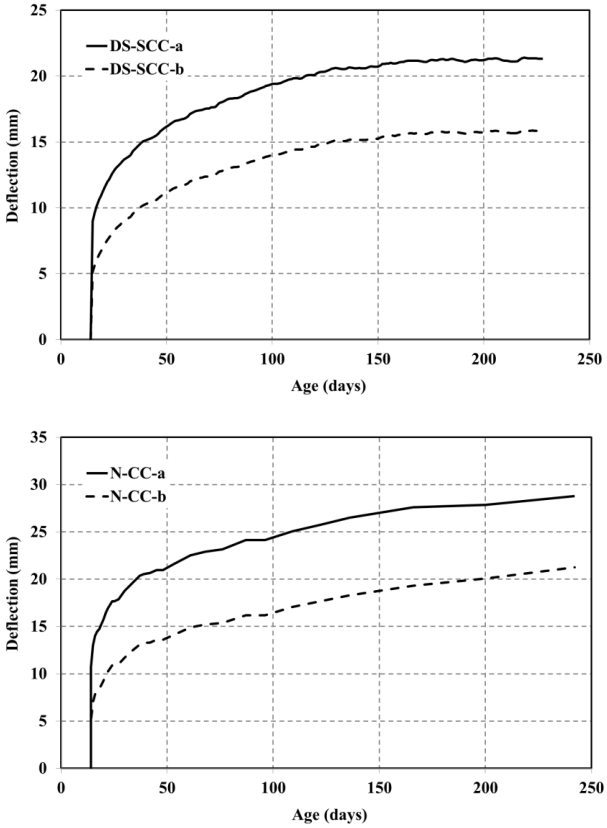

Fig. 5 Continued

0.07 mm for N-SCC-a and N-SCC-b, respectively. The instantaneous average crack spacing within this region were 147 mm and 138 mm, respectively. The measured maximum final crack widths at age 240 days within Region 2 were 0.24 mm and 0.18 mm for N-SCC-a and N-SCC-b, respectively, and the final average crack spacing were 123 mm and 100 mm respectively. The ratios of final to instantaneous crack spacing were 0.83 for N-SCC-a and 0.72 for N-SCC-b. The ratio of maximum final crack width to the final average crack width was 1.0 and 1.125 for N-SCC-a and N-SCC-b, respectively.

In Fig. 5 the measured deflections at the mid-span of slabs N-SCC-a and N-SCC-b versus time are illustrated. The measured long-term deflection of N-SCC-a and N-SCC-b at age 240 days were 24.75 mm and 18.08 mm respectively, which are 2.04 and 3.07 times the corresponding instantaneous deflections, respectively. The ratio of deflections at different ages to instantaneous deflection at mid-span for slabs N-SCC-a and N-SCC-b are presented in Table 7.

4.4.2 D-SCC slab series

Table 6 shows the long-term crack width history for slabs D-SCC-a and D-SCC-b. The measured maximum instantaneous crack widths within Region 2, were 0.09 mm and 0.07 mm for D-SCC-a and D-SCC-b, respectively. The instantaneous average crack spacing within this region were 124 mm and 131 mm, respectively. The measured maximum final crack widths at age 240 days within Region 2 were 0.22 mm and 0.14 mm for D-SCC-a and D-SCC-b, respectively, and

the final average crack spacing were 100 mm and 90 mm respectively. The ratios of final to instantaneous crack spacing were 0.80 for D-SCC-a and 0.68 for D-SCC-b. The ratio of maximum final crack width to the final average crack width was 1.0 and 1.076 for D-SCC-a and D-SCC-b, respectively.

In Fig. 5 the measured deflections at the mid-span of slabs D-SCC-a and D-SCC-b versus time are illustrated. The measured long-term deflection of D-SCC-a and D-SCC-b at age 240 days were 17.75 mm and 16.78 mm respectively, which are 2.32 and 2.21 times the corresponding instantaneous deflections, respectively. The ratio of deflections at different ages to instantaneous deflection at mid-span for slabs D-SCC-a and D-SCC-b are presented in Table 7.

4.4.3 S-SCC slab series

Table 6 shows the long-term crack width history for slabs S-SCC-a and S-SCC-b. The measured maximum instantaneous crack widths within Region 2, were 0.12 mm and 0.06 mm for S-SCC-a and S-SCC-b, respectively. The instantaneous average crack spacing within this region were 121 mm and 127 mm, respectively. The measured maximum final crack widths at age 240 days within Region 2 were 0.22 mm and 0.15 mm for S-SCC-a and S-SCC-b, respectively, and the final average crack spacing were 95 mm and 85 mm respectively. The ratios of final to instantaneous crack spacing were 0.78 for S-SCC-a and 0.68 for S-SCC-b. The ratio of maximum final crack width to the final average crack width was 1.1 and 1.0 for S-SCC-a and S-SCC-b, respectively.

In Fig. 5 the measured deflections at the mid-span of slabs S-SCC-a and S-SCC-b versus time are illustrated. The measured long-term deflection of S-SCC-a and S-SCC-b at age 240 days were 22.26 mm and 20.24 mm respectively, which are 3.47 and 6.95 times the corresponding instantaneous deflections, respectively. The ratio of deflections at different ages to instantaneous deflection at mid-span for slabs S-SCC-a and S-SCC-b are presented in Table 7.

4.4.4 DS-SCC slab series

Table 6 shows the long-term crack width history for slabs DS-SCC-a and DS-SCC-b. The measured maximum instantaneous crack widths within Region 2, were 0.10 mm and 0.06 mm for DS-SCC-a and DS-SCC-b, respectively. The instantaneous average crack spacing within this region were 129 mm and 133 mm, respectively. The measured maximum final crack widths at age 240 days within Region 2 were 0.20 mm and 0.14 mm for DS-SCC-a and DS-SCC-b, respectively, and the final average crack spacing were 102 mm and 88 mm respectively. The ratios of final to instantaneous crack spacing were 0.79 for DS-SCC-a and 0.66 for DS-SCC-b. The ratio of maximum final crack width to the final average crack width was 1.0 and 1.12 for DS-SCC-a and DS-SCC-b, respectively.

In Fig. 5 the measured deflections at the mid-span of slabs DS-SCC-a and DS-SCC-b versus time are illustrated. The measured long-term deflection of DS-SCC-a and DS-SCC-b at age 240 days were 21.30 mm and 15.83 mm respectively, which are 2.37 and 3.08 times the corresponding instantaneous deflections, respectively. The ratio of deflections at different ages to instantaneous deflection at mid-span for slabs DS-SCC-a and DS-SCC-b are presented in Table 7.

4.4.5 N-CC slab series

Table 6 shows the long-term crack width history for slabs N-CC-a and N-CC-b. The measured maximum instantaneous crack widths within Region 2, were 0.10 mm and 0.05 mm for N-CC-a

Table 6 Crack width at different regions for slab series

N-SCC-a		*t* = 0		*t* = 240 days	
M_{max}= 11.24 kNm	M (kNm)	Max.	Avge.	Max.	Avge.
$M \geq 0.99\ M_{max}$	11.13	0.11	0.11	0.24	0.24
$M \geq 0.90\ M_{max}$	10.12	0.10	0.10	0.23	0.23
$M \geq 0.80\ M_{max}$	8.99	0.10	0.09	0.22	0.20
$M \geq 0.70\ M_{max}$	7.87	0.10	0.09	0.20	0.19
N-SCC-b		*t* = 0		*t* = 240 days	
M_{max}= 11.24 kNm	M (kNm)	Max.	Avge.	Max.	Avge.
$M \geq 0.99\ M_{max}$	8.25	0.08	0.07	0.18	0.16
$M \geq 0.90\ M_{max}$	7.50	0.07	0.07	0.16	0.10
$M \geq 0.80\ M_{max}$	6.66	0.06	0.06	0.16	0.12
$M \geq 0.70\ M_{max}$	5.83	0.06	0.05	0.12	0.11
D-SCC-a		*t* = 0		*t* = 240 days	
M_{max}= 11.24 kNm	M (kNm)	Max.	Avge.	Max.	Avge.
$M \geq 0.99\ M_{max}$	11.13	0.11	0.11	0.22	0.22
$M \geq 0.90\ M_{max}$	10.12	0.09	0.09	0.18	0.18
$M \geq 0.80\ M_{max}$	8.99	0.09	0.08	0.16	0.15
$M \geq 0.70\ M_{max}$	7.87	0.08	0.07	0.14	0.14
D-SCC-b		*t* = 0		*t* = 240 days	
M_{max}= 11.24 kNm	8.25	-	-	-	-
$M \geq 0.99\ M_{max}$	7.50	0.07	0.065	0.14	0.13
$M \geq 0.90\ M_{max}$	6.66	0.06	0.055	0.12	0.11
$M \geq 0.80\ M_{max}$	5.83	0.06	0.055	0.10	0.10
$M \geq 0.70\ M_{max}$	8.25	-	-	-	-
S-SCC-a		*t* = 0		*t* = 240 days	
M_{max}= 11.24 kNm	M (kNm)	Max.	Avge.	Max.	Avge.
$M \geq 0.99\ M_{max}$	11.13	-	-	-	-
$M \geq 0.90\ M_{max}$	10.12	0.12	0.10	0.22	0.20
$M \geq 0.80\ M_{max}$	8.99	0.10	0.09	0.20	0.19
$M \geq 0.70\ M_{max}$	7.87	0.09	0.09	0.18	0.18
S-SCC-b		*t* = 0		*t* = 240 days	
M_{max}= 11.24 kNm	8.25	0.07	0.065	0.15	0.15
$M \geq 0.99\ M_{max}$	7.50	0.06	0.06	0.14	0.14
$M \geq 0.90\ M_{max}$	6.66	0.06	0.045	0.12	0.12
$M \geq 0.80\ M_{max}$	5.83	0.03	0.03	0.11	0.11
$M \geq 0.70\ M_{max}$	8.25	0.07	0.065	0.15	0.15

Table 6 Continued

DS-SCC-a		*t* = 0		*t* = 240 days	
M_{max}= 11.24 kNm	M (kNm)	Max.	Avge.	Max.	Avge.
M ≥ 0.99 M_{max}	11.13	0.10	0.10	0.20	0.20
M ≥ 0.90 M_{max}	10.12	-	-	-	-
M ≥ 0.80 M_{max}	8.99	0.10	0.09	0.20	0.19
M ≥ 0.70 M_{max}	7.87	0.08	0.075	0.18	0.17
DS-SCC-b		*t* = 0		*t* = 240 days	
M_{max}= 11.24 kNm	M (kNm)	Max.	Avge.	Max.	Avge.
M ≥ 0.99 M_{max}	8.25	-	-	-	-
M ≥ 0.90 M_{max}	7.50	0.06	0.055	0.14	0.125
M ≥ 0.80 M_{max}	6.66	0.05	0.05	0.12	0.12
M ≥ 0.70 M_{max}	5.83	0.05	0.045	0.11	0.105
N-CC-a		*t* = 0		*t* = 240 days	
M_{max}= 11.24 kNm	M (kNm)	Max.	Avge.	Max.	Avge.
M ≥ 0.99 M_{max}	11.13	0.10	0.10	0.25	0.17
M ≥ 0.90 M_{max}	10.12	0.10	0.09	0.2	0.15
M ≥ 0.80 M_{max}	8.99	0.08	0.07	0.18	0.15
M ≥ 0.70 M_{max}	7.87	0.05	0.05	0.18	0.14
N-CC-b		*t* = 0		*t* = 240 days	
M_{max}= 11.24 kNm	8.25	0.08	0.07	0.20	0.17
M ≥ 0.99 M_{max}	7.50	0.05	0.05	0.18	0.13
M ≥ 0.90 M_{max}	6.66	0.05	0.04	0.13	0.11
M ≥ 0.80 M_{max}	5.83	-	-	-	-
M ≥ 0.70 M_{max}	8.25	0.08	0.07	0.20	0.17

Table 7 Ratio of deflections at different ages to instantaneous deflection for slabs series

Age (days)	14	21	28	45	60	95	122	200	240
N-SCC-a	1.00	1.18	1.28	1.42	1.55	1.73	1.82	2.00	2.04
N-SCC-b	1.00	1.42	1.63	1.91	2.14	2.48	2.65	2.98	3.07
D-SCC-a	1.00	1.31	1.43	1.71	1.82	2.03	2.13	2.31	2.32
D-SCC-b	1.00	1.28	1.40	1.67	1.75	1.94	2.03	2.20	2.21
S-SCC-a	1.00	1.44	1.79	2.31	2.53	2.91	3.12	3.44	3.47
S-SCC-b	1.00	2.15	2.66	3.94	4.53	5.52	6.09	6.91	6.95
DS-SCC-a	1.00	1.30	1.48	1.72	1.89	2.13	2.26	2.36	2.37
DS-SCC-b	1.00	1.42	1.70	2.06	2.31	2.67	2.88	3.06	3.08
Age (days)	14	21	28	45	60	95	122	200	285
N-CC-a	1.00	1.54	1.67	1.96	2.10	2.25	2.40	2.61	2.72
N-CC-b	1.00	1.96	2.19	2.69	2.96	3.21	3.50	3.98	4.35

and N-CC-b, respectively. The measured maximum final crack widths at age 394 days within Region 2 were 0.25 mm and 0.20 mm for N-CC-a and N-CC-b, respectively, and the final average

crack spacing were 102 mm and 136 mm respectively. The ratios of final to instantaneous crack spacing were 0.67 for N-CC-a and 0.96 for N-CC-b. The ratio of maximum final crack width to the final average crack width was 1.47 and 1.17 for N-CC-a and N-CC-b, respectively. In Fig. 5 the measured deflections at the mid-span of slabs N-CC-a and N-CC-b versus time are illustrated. The measured long-term deflection of N-CC-a and N-CC-b at age 285 days were 32.10 mm and 21.92 mm respectively, which are 2.75 and 4.54 times the corresponding instantaneous deflections, respectively. The ratio of deflections at different ages to instantaneous deflection at mid-span for slabs N-CC-a and N-CC-b are presented in Table 7.

5. Discussion on the experimental results

5.1 Cracking behaviour

As Table 8 shows, instantaneous minimum, average, and maximum crack widths for N-SCC slab series are close to N-CC slab series and instantaneous average spacing of N-SCC-a slab is 54 mm less than N-CC-a and instantaneous average spacing of N-SCC-b slab is 41 mm less than N-CC-b. Moreover, time-dependent minimum, average, and maximum crack widths for N-SCC-a slab are slightly more than N-CC-a slab but crack widths for N-SCC-b slab are slightly less than N-CC-b slab. Also, time-dependent average spacing of N-SCC-a slab is 5 mm less than N-CC-a and time-dependent average spacing of N-SCC-b slab is 41 mm less than N-CC-b. These results are shown that crack spacing by using SCC is much less than CC.

About the other SCC mixtures, instantaneous minimum, average, and maximum crack widths for D-SCC, S-SCC, and DS-SCC slab series are close to N-SCC and N-CC slab series crack widths. But, time-dependent minimum, average, and maximum crack widths for D-SCC, S-SCC, and DS-SCC slab series are slightly less than N-SCC slab series and are close to N-CC slab series crack widths. Also, same as N-SCC slab series, other SCC mixture slab series average crack spacing are much higher than N-SCC slab series average crack spacing.

5.2 Deflection

The results of slab series N-SCC and N-CC show that the slab series N-SCC's instantaneous deflection is close to N-CC but the final deflections of N-SCC slab series are less than N-CC slab series. The final deflection of N-SCC-a is 7.5 mm less than N-CC-a and the final deflection of N-SCC-b is 3.8 mm less than N-CC-b. About the instantaneous deflection of the other SCC mixtures slab series, all of them are less than N-SCC and N-CC slab series. Also, the S-SCC slab series instantaneous deflections surprisingly are less than the other SCC slab series instantaneous deflections. About the final deflection, the D-SCC slab series have the minimum final deflections compare to the all other slab series.

The D-SCC-a final deflection is 7 and 14.3 mm is less than the N-SCC-a and N-CC-a slabs and the D-SCC-b final deflection is 1.3 and 5.1 mm is less than the N-SCC-b and N-CC-b slabs. The main reason for this reduction of final deflection is using steel fibre in the mixture. After the D-SCC minimum final deflection, DS-SCC slab series hold the less final defections compare to the N-SCC, N-CC, and S-SCC slab series.

6. Time-dependent bond shear stress

The force in the bar is transmitted to the surrounding concrete by bond shear stress τ_b. Due to this transfer, the force in a reinforcing bar changes along its length. The transfer of forces across the interface by bond between concrete and steel is of fundamental importance to many aspects of reinforced concrete behaviour.

Under service conditions $\sigma_s < f_{sy}$ and according to Marti *et al*. (1998), $\tau_b = 2\ f_{ct}$. Following the CEB proposal which accounts for the breakdown of tension stiffening under long-term or cyclic loading, each value was reduced by a factor of one half ($\tau_b(t) = 0.5\ f_{ct}$, $\tau_b(t) = f_{ct}$ and $\tau_b(t) = 1.5\ f_{ct}$) for time-dependent behaviour. Time-dependent crack width calculations for concrete reinforced with bars only are different from concrete reinforced with bars and fibres, as described in sections 6.1 and 6.2.

6.1 Crack width calculations of steel bar reinforcement concrete

Maximum crack width calculation for long-term behaviour can be presented as follows: Under sustained load, additional cracks occur between widely spaced cracks (usually when $0.67 s_{max} < s \leq s_{max}$). The additional cracks are due to the combined effect of tensile creep rupture and shrinkage. As a consequence, the number of cracks increases and the maximum crack spacing reduces with time. The final maximum crack spacing, s^* is only about two-thirds of that given by Eq. (1), but the final minimum crack spacing remains about half of the value given by Eq. (1).

$$s_{\max} = \frac{f_{ct}\ d_b}{2\ \tau_b\ \rho_{tc}} \tag{1}$$

where ρ_{tc} is the reinforcement ratio of the tension chord (= A_{st}/A_{ct}), d_b is the reinforcing bar diameter, τ_b is the bond stress, f_{ct} is the direct tensile strength of the concrete.

Table 8 Summary of the results from long-term flexural test

Specimen	Instantaneous				Time-dependent				$(s_{rm})_{final} / (s_{rm})_{inst.}$
	w_{min} (mm)	w_{ave} (mm)	w_{max} (mm)	$s_{rm,ave}$ (mm)	w_{min} (mm)	w_{ave} (mm)	w_{max} (mm)	$s_{rm,ave}$ (mm)	
N-SCC-a	0.03	0.07	0.11	99	0.06	0.15	0.24	97	0.98
N-SCC-b	0.03	0.05	0.08	100	0.03	0.11	0.18	95	0.95
D-SCC-a	0.04	0.07	0.11	96	0.06	0.13	0.22	95	0.99
D-SCC-b	0.02	0.05	0.07	99	0.02	0.09	0.14	95	0.96
S-SCC-a	0.03	0.07	0.12	96	0.07	0.15	0.22	94	0.98
S-SCC-b	0.02	0.04	0.07	93	0.05	0.10	0.15	91	0.98
DS-SCC-a	0.03	0.06	0.10	102	0.04	0.14	0.20	98	0.96
DS-SCC-b	0.02	0.04	0.06	94	0.04	0.09	0.14	90	0.96
N-CC-a	0.05	0.09	0.10	153	0.10	0.15	0.22	102	0.67
N-CC-b	0.03	0.04	0.08	141	0.08	0.14	0.20	136	0.96

Nejadi (2005) is presented that experimental observations indicate that τ_b decreases with time, probably as a result of shrinkage-induced slip and tensile creep. Hence, the stress in the tensile concrete between the cracks gradually reduces. Furthermore, although creep and shrinkage will cause a small increase in the resultant tensile force T in the real beam and a slight reduction in the internal lever arm, this effect is relatively small and is ignored in the tension chord model presented here. The final crack width is the elongation of the steel over the distance between the cracks minus the extension of the concrete caused by σ_{cz} plus the shortening of the concrete between the cracks due to shrinkage. For a final maximum crack spacing of s^*, the final maximum crack width at the member soffit is:

$$\left(w^*\right)_{soffit} = \frac{s^*}{E_s}\left[\frac{T}{A_{st}} - \frac{\tau_b\, s^*}{d_b}\left(1 + n_e\, \rho_{tc}\right) - \varepsilon_{sh}\, E_s\right] \tag{2}$$

$$n_e = \frac{E_s}{E_e} \tag{3}$$

$$E_e = \frac{E_c}{\left(1 + \varphi(t,\tau)\right)} \tag{4}$$

where ε_{sh} is the shrinkage strain in the tensile concrete (and is a negative value), A_{st} is the tensile reinforcement of area, E_c and E_s are the elastic moduli of the concrete and steel respectively, and $\varphi(t,\tau)$ is the creep coefficient of the concrete.

6.2 Crack width calculations of steel bar reinforcement concrete with fibres

Maximum crack width calculation for long-term behaviour is presented by Leutbecher and Fehling (2008). They have derived a cracking behaviour model based on the assumptions of constant bond stress and a parabolic development of concrete and steel strains between the cracks (refer to Fig. 6):

$$\begin{aligned} w_s &= s_r\left(\varepsilon_{sm} - \varepsilon_{cm}\right) = \\ & s_r\left[\frac{\sigma_s}{E_s} - \alpha_b\left(\frac{2\, s_r\, \tau_{sm}}{d_s\, E_s}\left(1 + \alpha_{E,s}\, \rho_s / \gamma\right) + \frac{\sigma_{cf}}{\gamma\, E_s}\,\alpha_{E,s} - \varepsilon^*_{f,shr}\,\alpha_{E,f}\,\eta\,\rho_f\right) - \varepsilon^*_{shr}\right] \end{aligned} \tag{5}$$

$$s_{r,max} = \left(\sigma^i_{cf,cr} - \sigma_{cf0}\right)\frac{d_s}{2\,\tau_{sm}\,\rho_s} \tag{6}$$

$$\varepsilon^*_{shr} = \varepsilon_{s,shr}\left(1 + \alpha_{E,s}\,\rho_s/\gamma\right) + \varepsilon_{f,shr}\,\alpha_{E,f}\,\eta\,\rho_f \tag{7}$$

$$\varepsilon^*_{f,shr} = \varepsilon_{f,shr}\,\gamma \tag{8}$$

$$\gamma = 1 + \rho_f\left(\eta\,\alpha_{E,f} - 1\right) \tag{9}$$

where σ_{cf} is the stress in the fibre reinforced concrete (Eqs. 10 and 11), $\varepsilon_{f,shr}$ is the shrinkage shortening of the fibres, τ_{sm} is the average bond stress over load transmission length, d_b is the reinforcing bar diameter, E_s is the modulus of elasticity of reinforcing bar, ρ_s is the reinforcing

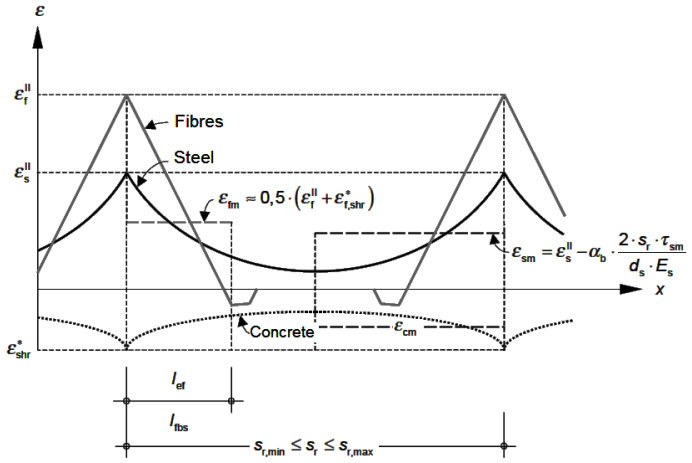

Fig. 6 Stabilized cracking - Qualitative distribution of strains for the bar and fibres reinforcement and for the matrix, considering the influence of shrinkage

ratio of steel reinforcement, ρ_f is the fibre content, η is the fibre orientation coefficient; α_b is the shape coefficient of strain courses (α_b = 0.6 for short term loading, α_b = 0.4 for long term or repeated loading); $\alpha_{E,s}$ is the ratio of the modulus of elasticity of steel to the modulus of elasticity of concrete. $\alpha_{E,s} = E_s/E_c$; $\alpha_{E,f}$ is the ratio of the modulus of elasticity of fibre to the modulus of elasticity of concrete. $\alpha_{E,f} = E_f/E_c$. Refer to Fig. 6 for definitions of the various stresses used in this model.

$$\sigma_{cf} = f_{ct}\left(1-\frac{w\,f_{ct}}{2G_f}\right)+\sigma_{cf\,0}\left(2\sqrt{\frac{w}{w_0}}-\frac{w}{w_0}\right) \tag{10}$$

where w is the crack width, f_{ct} is the concrete matrix tensile strength, G_f is the fracture energy of the concrete matrix, σ_{cf0} is the maximum post-cracking stress, w_0 is the crack width corresponding to maximum post-cracking stress, mm.

During the fibre pullout phase, the fibre stress can be calculated from the following equation:

$$\sigma_{cf} = \sigma_{cf\,0}\left(1-\frac{w}{l_f}\right) \tag{11}$$

where σ_{cf0} is the maximum post-cracking stress. The σ_{cf0} for fibres with a random orientation, it can be calculated as:

$$\sigma_{cf\,0} = \eta\, g\, \rho_f\, \frac{\tau_{fm}\, l_f}{d_f} \tag{12}$$

where η is the coefficient of fibre orientation; g is the coefficient of fibre efficiency (i.e. – damage factor), ρ_f is the volume fraction of fibres, l_f is the fibre length, d_f is the fibre diameter, τ_{fm} is the mean fibre-matrix bond stress. The mean fibre-matrix bond stress can be approximated as:

$$\tau_{fm} = 1.3\, f_{ctm} \tag{13}$$

where f_{ctm} is the mean tensile strength of the plain concrete matrix.

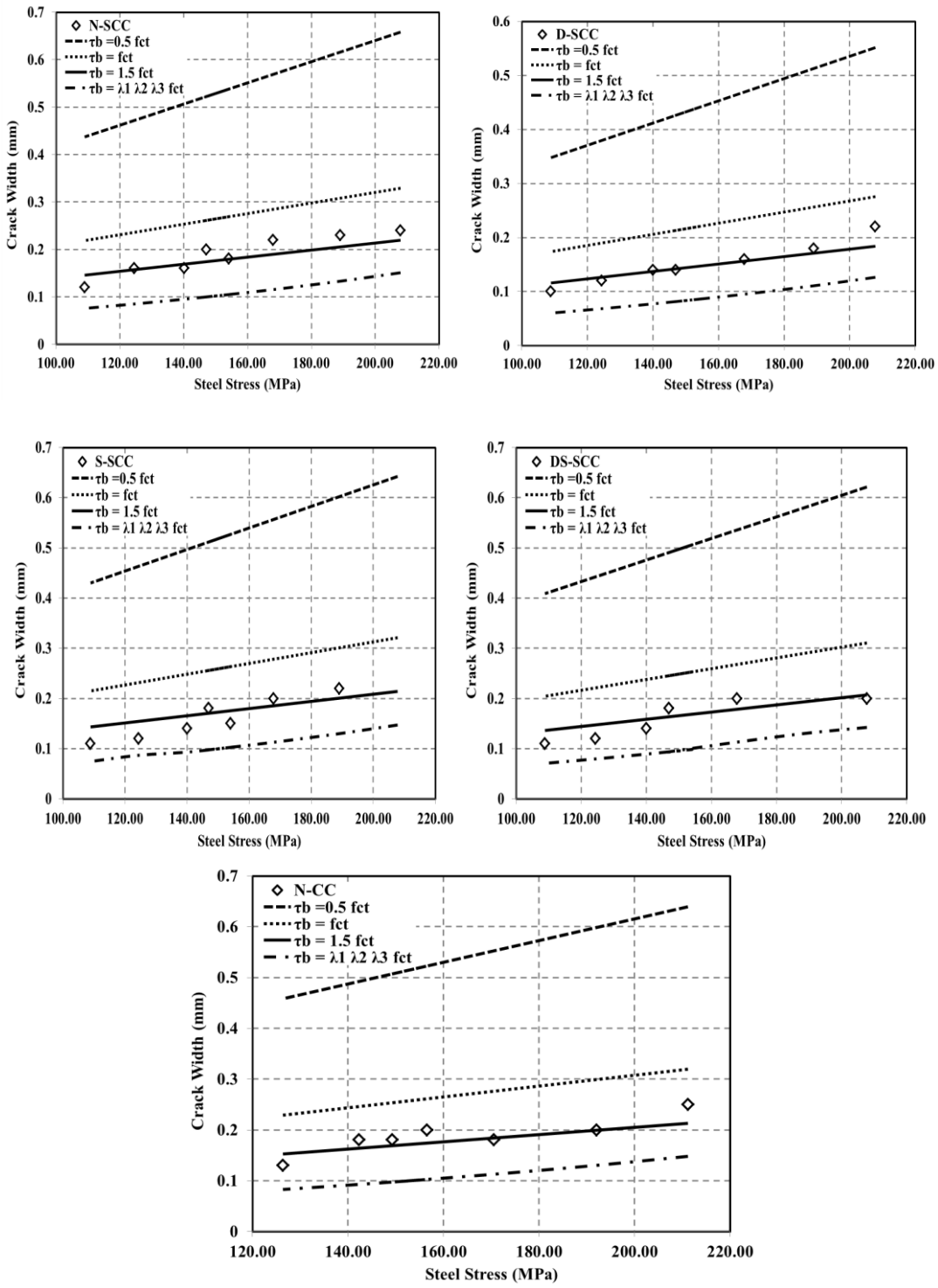

Fig. 7 Comparison of different bond stresses for SCC and N-CC slab series

6.3 Crack width calculations with different bond shear stress

For N-SCC mix, Eq.(2) is used for time-dependent crack width calculations and for D-SCC, S-SCC, and DS-SCC mixes, Eq.(5) is used. The results are presented in Tables 9-13. Measured and calculated maximum crack widths versus steel stress are illustrated in Fig. 7.

Table 9 Measured and calculated maximum crack width for slab N-SCC series

	N-SCC			Bond Stress			
	M (kNm)	σ_{st} (MPa)	Experiment w_{max} (mm)	$\tau_b = 0.5\ f_{ct}$	$\tau_b = f_{ct}$	$\tau_b = 1.5\ f_{ct}$	$\tau_b = \lambda_1\ \lambda_2\ \lambda_3\ f_{ct}$
				w_{max} (mm)			
N-SCC-a	11.13	207.94	0.24	0.658	0.329	0.219	0.151
	10.12	189.07	0.23	0.616	0.308	0.205	0.133
	8.99	167.96	0.22	0.569	0.284	0.190	0.115
	7.87	147.03	0.20	0.522	0.261	0.174	0.100
N-SCC-b	8.25	154.13	0.18	0.538	0.269	0.179	0.105
	7.50	140.12	0.16	0.507	0.253	0.169	0.095
	6.66	124.43	0.16	0.472	0.236	0.157	0.085
	5.83	108.92	0.12	0.437	0.219	0.146	0.076

Table 10 Measured and calculated maximum crack width for slab D-SCC series

	D-SCC			Bond Stress			
	M (kNm)	σ_{st} (MPa)	Experiment w_{max} (mm)	$\tau_b = 0.5\ f_{ct}$	$\tau_b = f_{ct}$	$\tau_b = 1.5\ f_{ct}$	$\tau_b = \lambda_1\ \lambda_2\ \lambda_3\ f_{ct}$
				w_{max} (mm)			
D-SCC-a	11.13	207.85	0.22	0.552	0.276	0.184	0.126
	10.12	188.99	0.18	0.513	0.256	0.171	0.111
	8.99	167.88	0.16	0.469	0.235	0.156	0.095
	7.87	146.97	0.14	0.426	0.213	0.142	0.081
D-SCC-b	8.25	154.06	-	0.441	0.220	0.147	0.086
	7.50	140.06	0.14	0.412	0.206	0.137	0.077
	6.66	124.37	0.12	0.380	0.190	0.127	0.068
	11.13	207.85	0.22	0.552	0.276	0.184	0.126

Table 11 Measured and calculated maximum crack width for slab S-SCC series

	S-SCC			Bond Stress			
	M (kNm)	σ_{st} (MPa)	Experiment w_{max} (mm)	$\tau_b = 0.5\ f_{ct}$	$\tau_b = f_{ct}$	$\tau_b = 1.5\ f_{ct}$	$\tau_b = \lambda_1\ \lambda_2\ \lambda_3\ f_{ct}$
				w_{max} (mm)			
S-SCC-a	11.13	207.85	-	0.642	0.321	0.214	0.147
	10.12	188.99	0.22	0.602	0.301	0.201	0.130
	8.99	167.88	0.20	0.557	0.278	0.186	0.113
	7.87	146.97	0.18	0.512	0.256	0.171	0.098
S-SCC-b	8.25	154.06	0.15	0.527	0.264	0.176	0.103
	7.50	140.06	0.14	0.497	0.249	0.166	0.093
	6.66	124.37	0.12	0.463	0.232	0.154	0.116
	5.83	108.87	0.11	0.430	0.215	0.143	0.074

Table 12 Measured and calculated maximum crack width for slab DS-SCC series

	DS-SCC			Bond Stress			
	M (kNm)	σ_{st} (MPa)	Experiment w_{max} (mm)	$\tau_b = 0.5\ f_{ct}$	$\tau_b = f_{ct}$	$\tau_b = 1.5\ f_{ct}$	$\tau_b = \lambda_1\ \lambda_2\ \lambda_3\ f_{ct}$
				w_{max} (mm)			
DS-SCC-a	11.13	207.77	0.20	0.621	0.311	0.207	0.142
	10.12	188.91	-	0.581	0.291	0.194	0.131
	8.99	167.82	0.20	0.536	0.268	0.179	0.113
	7.87	146.91	0.18	0.491	0.245	0.164	0.094
DS-SCC-b	8.25	154.00	-	0.506	0.253	0.169	0.099
	7.50	140.00	0.14	0.476	0.238	0.159	0.089
	6.66	124.32	0.12	0.442	0.221	0.147	0.080
	5.83	108.83	0.11	0.409	0.205	0.136	0.071

Table 13 Measured and calculated maximum crack width for slab N-CC series

	N-CC			Bond Stress			
	M (kNm)	σ_{st} (MPa)	Experiment w_{max} (mm)	$\tau_b = 0.5\ f_{ct}$	$\tau_b = f_{ct}$	$\tau_b = 1.5\ f_{ct}$	$\tau_b = \lambda_1\ \lambda_2\ \lambda_3\ f_{ct}$
				w_{max} (mm)			
N-CC-a	11.13	211.18	0.25	0.639	0.320	0.213	0.148
	10.12	192.01	0.20	0.598	0.299	0.199	0.130
	8.99	170.57	0.18	0.553	0.276	0.184	0.113
	7.87	149.32	0.18	0.507	0.254	0.169	0.098
N-CC-b	8.25	156.53	0.20	0.523	0.261	0.174	0.103
	7.50	142.30	0.18	0.492	0.246	0.164	0.093
	6.66	126.36	0.13	0.458	0.229	0.153	0.083

6.4 Adopted bond shear stress for crack width calculation of SCC slabs

Three different values for bond shear stress ($\tau_b(t) = 0.5\ f_{ct}$, $\tau_b(t) = f_{ct}$ and $\tau_b(t) = 1.5\ f_{ct}$) have been considered and the corresponding crack widths were calculated and compared with the experimental results for each load increment. It should be mentioned that throughout the test, crack widths were monitored at two levels on the side of each specimens, i.e., the steel level and bottom fibre. Considering this and comparing the best fit between the calculated values and measured crack widths, the expressions for the bond shear stress τ_b for SCC slab series are presented in Eq. (14) and Fig. 7, under long-term loading and for the different in-service steel stress ranges have been adopted for the analytical model.

$$\tau_b = 1.5\ f_{ct} \tag{14}$$

Presented Eq. (14) is based on the comprehensive analyses and comparisons that are summarized and presented in Fig. 7.

7. Conclusions

The following conclusions can be drawn from this experimental study:

- Instantaneous crack widths for N-SCC slab series are close to N-CC slab series but instantaneous average spacing of N-SCC slab series are much less than N-CC slab series.
- Time-dependent crack widths for N-SCC-a slab are slightly more than N-CC-a slab but crack widths for N-SCC-b slab are slightly less than N-CC-b slab. Also, time-dependent average spacing of N-SCC slab series are much less than N-CC slab series.
- The DS-SCC slab series are shown the minimum instantaneous and time-dependent crack widths compare to the other mixtures slab series.
- The S-SCC slab series instantaneous deflections are surprisingly less than the other SCC slab series.
- The slab series N-SCC's instantaneous deflection is close to N-CC but the final deflections of N-SCC slab series are less than N-CC slab series. Also, the instantaneous deflections of other SCC mixtures slab series are less than N-SCC and N-CC slab series.
- The D-SCC slab series have the minimum final deflections compare to the all other slab series. The main reason for this reduction of final deflection is using steel fibre in the mixture.
- The presented experimental results can assist in the development of rational design-oriented procedures for the control of cracking and the calculation of crack widths in reinforced SCC and FRSCC slabs.
- The comparisons confirm that the proposed bond shear stress for CC is suitable for SCC slab series. Furthermore, the calculated crack widths by using the $\tau_b = 1.5\ f_{ct}$ bond shear stress are suitable for all of SCC slab series.
- The crack widths calculated by using adopted bond shear stresses for SCC and FRSCC slabs are in good agreement with experimental results.

Acknowledgements

This work was supported by Centre for Built Infrastructure Research, School of Civil and Environmental Engineering, University of Technology Sydney, Australia. The authors would like to express their sincere gratitude and appreciation to Boral, BOSFA, and Concrite companies.

References

Abrishami, H.H. and Mitchell, D. (1997), "Influence of steel fibers on tension stiffening", *ACI Struct. J.*, **94**, 769-775.

ACI 232.2R-03 (2004), "Use of fly ash in concrete", ACI Committee 232.

ACI 233R-95 (2000), "Ground granulated blast-furnace slag as a cementitious constituent in concrete," ACI Committee 233.

ACI 237R-07 (2007), "Self-Consolidating Concrete", ACI Committee 237.

ACI 544.2R (1999), *State-of-the-Art Report on Fiber Reinforced Concrete*, Technical report, American Concrete Institute.

Arici, M. and Granata, M.F. (2013), "Conceptual design of prestressed slab bridges through one-way flexural load balancing", *Struct. Eng. Mech.*, **48**(5), 615-642.

AS 1012.14 (1991), "Method for securing and testing from hardened concrete for compressive strength".

AS 1012.13 (1992), "Determination of the drying shrinkage of concrete for samples prepared in the field or

in the laboratory".
AS 1012.16 (1996), "Determination of creep of concrete cylinders in compression. Standards Australia".
AS 1012.17 (1997), "Determination of the static chord modulus of elasticity and Poisson's ratio of concrete specimens".
AS 1141 (2011), "Methods for sampling and testing aggregates - Particle size distribution - Sieving method", Standards Australia.
AS 1478.1. (2000), "Chemical admixtures for concrete, mortar and grout - Admixtures for concrete", Standards Australia.
AS 2350 (2006), "Methods of testing portland and blended cements", Standards Australia.
AS 3582.2 (2001), "Supplementary cementitious materials for use with portland and blended cement - Slag - Ground granulated iron blast-furnace", Standards Australia.
AS 3583 (1998), "Methods of test for supplementary cementitious materials for use with portland cement", Standards Australia.
AS 3972. (2010), "General purpose and blended cements", Standards Australia.
Aslani, F. and Nejadi, S. (2012a), "Mechanical properties of conventional and self-compacting concrete: An analytical study", *Constr. Build. Mater.*, **36**, 330-347.
Aslani, F. and Nejadi, S. (2012b), "Bond characteristics of steel fibre reinforced self-compacting concrete", *Can. J. Civil. Eng.*, **39**(7), 834-848.
Aslani, F. and Nejadi, S. (2012c), "Bond behavior of reinforcement in conventional and self-compacting concrete", *Adv. Struct. Eng.*, **15**(12), 2033-2051.
Aslani, F. and Nejadi, S. (2012d), "Shrinkage behavior of self-compacting concrete", *J. Zhejiang Uni. Sci. A*, **13**(6), 407-419.
Aslani, F. and Nejadi, S. (2012e), "Bond characteristics of Reinforcing Steel Bars Embedded in Self-Compacting Concrete", *Aust J. Struct. Eng.*, **13**(3), 279-295.
Aslani, F. and Nejadi, S. (2013a), "Self-compacting concrete incorporating steel and polypropylene fibers: compressive and tensile strengths, moduli of elasticity and rupture, compressive stress-strain curve, and energy dissipated under compression", *Compos. Part B-Eng.*, **53**, 121-133.
Aslani, F. and Nejadi, S. (2013b), "Creep and shrinkage of self-compacting concrete with and without Fibers", *J Adv. Concr. Technol.*, **11**(10), 251-265.
Aslani, F. (2013), "Effects of Specimen Size and Shape on Compressive and Tensile Strengths of Self-Compacting Concrete with or without Fibers", *Mag. Concrete Res.*, **65**(15), 914-929.
Aslani, F. and Maia, L. (2013), "Creep and Shrinkage of High Strength Self-Compacting Concrete Experimental and Numerical Analysis", *Mag. Concrete Res.*, **65**(17), 1044-1058.
Aslani, F. and Natoori, M. (2013), "Stress-strain relationships for steel fibre reinforced self-compacting concrete", *Struct. Eng. Mech.*, **46**(2), 295-322.
Aslani, F., Nejadi, S. and Samali, B. (2014), "Short term bond shear stress and cracking cntrol of reinforced self-compacting concrete one way slabs under flexural loading", *Comput. Concrete*, **13**(6), 709-737.
Aslani, F. and Samali, B. (2014), "Flexural toughness characteristics of self-compacting concrete incorporating steel and polypropylene fibers", *Aust. J. Struct. Eng.*, **15**(3), 269-286.
ASTM standards (2000), Volume 04.02, "Concrete and aggregates".
ASTM C183-08 (2000), "Standard Practice for Sampling and the Amount of Testing of Hydraulic Cement", ASTM standards 2000 (Annual book).
ASTM C31 -11b (2000), "Standard Test Methods for Sampling and Testing Fly Ash or Natural Pozzolans for Use in Portland-Cement Concrete", ASTM standards 2000 (Annual book), 2000.
ASTM C989-06 (2000), "Standard Specification for Ground Granulated Blast-Furnace Slag for Use in Concrete and Mortars", ASTM standards 2000 (Annual book).
ASTM C1077-13 (2000), "Standard Practice for Agencies Testing Concrete and Concrete Aggregates for Use in Construction and Criteria for Testing Agency Evaluation", ASTM standards 2000.
Balazs, G.L. and Kovacs, I. (2004), "Effect of steel fibers on the cracking behaviour of RC members," In: Proceedings of 6th RILEM symposium on fiber-reinforced concretes – BEFIB 2004, Varenna, Italy.
Bishoff, P.H. (2003), "Tension stiffening and cracking of steel fiber reinforced concrete", *J. Mater. Civ.*

Eng., **15**(2), 174-182.
Buratti, N., Mazzotti, C. and Savoia, M. (2010), "Long-term behaviour of fibre-reinforced self-compacting concrete beams", Design, Production and Placement of Self-Consolidating Concrete, SCC2010, Montreal, Canada, 1, 439-450.
Chen, H.J., Tsai, W.P., Tang, C.W. and Liu, T.H. (2011), "Time-dependent properties of lightweight concrete using sedimentary lightweight aggregate and its application in prestressed concrete beams," *Struct. Eng. Mech.*, **39**(6), 833-847.
Chiaia, B., Fantilli, A.P. and Vallini, P. (2008), "Crack patterns in reinforced and fiber reinforced concrete structures", *Open Constr. Build. Technol. J.*, **2**, 146-155.
European guidelines (2005), "The european guidelines for self-compacting concrete, Specification, production and use".
Leutbecher, T. and Fehling, E. (2008), "Crack formation and tensile behaviour of UHPC reinforced with a combination of rebars and fibres", In: Schmidt, M., Fehling, E., Stürwald, S. (Eds.) Ultra High Performance Concrete (UHPC), Second International Symposium on Ultra High Performance Concrete, *Struct. Mater. Eng. Series*, **10**, 497-504.
Marti, P., Alvarez, M., Kaufmann, W. and Sigrist, V. (1998), "Tension chord model for structural concrete," *Struct. Eng. Int.*, **4**, 287-298.
Mazzotti, C. and Savoia, M. (2009), "Long-term deflection of reinforced self-consolidating concrete beams", *ACI Struct. J.*, **6**(6), 772-781.
Minelli, F., Tiberti, G. and Plizzari, G. (2010), "Durability and cracking in fibrous R/C elements: a broad experimental study," Atti del Convegno Le Nuove Frontiere del Calcestruzzo Strutturale, Università degli Studi di Salerno – ACI Italy.
Nejadi, S. (2005), "Time-dependent cracking and crack control in reinforced concrete structures", Ph.D. Thesis, The University of New South Wales.
Oh, B.H. (1992), "Flexural analysis of reinforced concrete beams containing steel fibers", *J Struct. Eng.*, **118**, 2821-2836.
RILEM TC 162-TDF (2002), "Test and design methods for steel fibre reinforced concrete", Final recommendations, *Mater. Struct.*, **35**, 579-582.
RTA (Regional Transportation Authority) (2006), "Materials test methods", Vol. 1.
Tan, K.H., Paramasivam P. and Tan K.C. (1995), "Cracking characteristics of reinforced steel fiber concrete beams under short and long-term loadings", *Adv. Cem. Mater.*, **2**, 127-137.
Tan, K.H. and Saha, M.K. (2005), "Ten-year study on steel fiber-reinforced concrete beams under sustained loads", *ACI Struct. J*, **102**(3), 472-480.
Vandewalle, L. (2000), "Cracking behavior of concrete beams reinforced with a combination of ordinary reinforcement and steel fibers", *Mater. Struct*, **33**, 164-170.
Wu, H.Q. and Gilbert, R.I. (2009), "Modelling short-term tension stiffening in reinforced concrete prisms using a continuum-based finite element model", *Eng. Struct.*, **31**(10), 2380-2391.
Xiao-jie, L., Zhi-wu, Y. and Li-zhong, J. (2008), "Long term behavior of self-compacting reinforced concrete beams", *J. Cent. South Uni. Tech.*, **15**(3), 423-428.

CC